Petroleum Science 20 (2023) 350–361

Contents lists available at ScienceDirect

Petroleum Science

journal homepage: www.keaipublishing.com/en/journals/petroleum-science

Original Paper

# Further discussion of $CO_2$ huff-n-puff mechanisms in tight oil reservoirs based on NMR monitored fluids spatial distributions

Wei-Yu Tang [a], James J. Sheng [b, *], Ting-Xue Jiang [c]

[a] Unconventional Petroleum Research Institute, China University of Petroleum, Beijing, 102249, China
[b] Bob L. Herd Department of Petroleum Engineering, Texas Tech University, Lubbock, TX, 79409, USA
[c] Sinopec Research Institute of Petroleum Engineering, Beijing, 100101, China

ARTICLE INFO

*Article history:*
Received 22 February 2022
Received in revised form
29 July 2022
Accepted 13 August 2022
Available online 23 August 2022

Edited by Yan-Hua Sun

*Keywords:*
Tight reservoirs
Low-field nuclear magnetic resonance (NMR)
$CO_2$ huff-n-puff
Enhanced oil recovery

ABSTRACT

Due to the poor physical properties of tight reservoirs, $CO_2$ huff-n-puff (HNP) is considered a potential enhanced oil recovery (EOR) method after primary depletion. Optimization plays a critical role in the effective implementation of $CO_2$ huff-n-puff. But the optimization requires a good understanding of the EOR mechanisms. In this work, the spatial distribution of oil saturation under different experimental conditions was analyzed by the NMR method to further discuss the HNP mechanisms. According to the variation of 1D frequency signal amplitude, we divided the core into the hardly movable area and movable area, the region with the obvious signal decline was defined as the movable area, and the hardly movable area was the region with limited signal decline. Based on that the recovery characteristics of different scenarios were evaluated. Firstly, the necessity of the soaking stage was studied, where three scenarios with different soaking times were carried out. Secondly, the injection pressure was adjusted to investigate the effect of the pressure gradient. The $T_2$ spectra show that soaking has significantly improved the production of crude oil in small pores, and higher oil recovery in a single cycle is observed, but it is lower when the elapsed time (total operation time) is the same. 31.03% of oil can be recovered after 3 cycles HNP, which increases to 33.8% and 37.06% for the 4 cycles and 6 cycles cases. As the pressure gradient increases, more oil is removed out of the matrix, and the oil in the deep part of the reservoir can be effectively recovered. During the $CO_2$ huff-n-puff process, the oil distributions are similar to the solution gas drive, the residual oil is distributed at the close end of the core and the range that the oil can be efficiently recovered is limited.


## 1. Introduction

With the decreasing amount of recoverable conventional resources, tight reservoirs that were unprofitable in the past decades have been drawing increasing worldwide attention (Zou et al., 2014, 2015; Pang et al., 2012). However, the extremely low porosity and permeability in tight formation have caused the conventional development methods to encounter great challenges. Even with the combination of horizontal well drilling and multi-stage fracturing, the recovery of primary depletion is under 10%, which has a great potential for enhanced tight oil recovery (Ma et al., 2015; Sheng, 2015b, 2017a). Water injection has achieved great success in conventional reservoirs. However, introducing water into the tight formation may cause several problems (Zhou et al., 2020), lower pressure transmission efficiency (Duan and Yang, 2014), and physical changes in the formation may have uncertain effects during the water treatment process (Qin et al., 2015). Compared with water, $CO_2$ is easier to inject, causing less damage to the reservoir, and has a better recovery efficiency in tight reservoirs (Sheng and Chen, 2014). More particularly, $CO_2$ is classified as the main greenhouse gas, and its massive emissions into the atmosphere can cause adverse environmental impacts, especially global warming (Abedini and Torabi, 2014; Cuéllar-Franca and Azapagic, 2015). Effective use of $CO_2$ can not only obtain additional economic benefits but also help reduce the concentration of $CO_2$ in the atmosphere by permanently storing $CO_2$ underground (Li Q. et al., 2016; Bachu, 2016).

* Corresponding author.
*E-mail address:* james.sheng@ttu.edu (J.J. Sheng).

https://doi.org/10.1016/j.petsci.2022.08.014

**Nomenclature**

| | |
|---|---|
| HNP | Huff-n-Puff |
| EOR | Enhanced oil recovery |
| NMR | Nuclear magnetic resonance |
| GR-HSE | Gradient hard spin echo |
| CPMG | Carr-Purcell-Meiboom-Gill spin echo |
| MRI | Magnetic resonance imaging |
| $T_2$ | Transverse relaxation time |
| TE | Echo time |
| TR | Repetition time |
| PDP | Pulse decay permeability |
| OOIP | Original oil in place |

Many studies have shown their confidence in the $CO_2$-based EOR method in tight reservoirs. Yu et al. (2021) investigated the feasibility of several $CO_2$-based flooding methods and proposed that activated carbonated water alternating gas injection has the highest oil recovery. Due to the poor pressure propagated efficiency and gas breakthrough problem, gas flooding has had limited success in the EOR application of tight reservoirs. Chen et al. (2014) proposed that it is difficult for injection pressure to effectively transmit to the producer by traditional flooding methods, $CO_2$ huff-n-puff (HNP) has been considered a potential method to enhance oil recovery in tight reservoirs. Different from gas flooding, HNP can periodically restore formation pressure, which has higher EOR potential. Zuloaga et al. (2017) set up a field-scale numerical model of the Middle Bakken formation and performed a comparison of $CO_2$ HNP and $CO_2$ flooding. HNP performs better when the permeability is less than 0.03 mD, they indicated that matrix permeability is the most sensitive parameter for the comparison of HNP and flooding, followed by well pattern and the interaction between fracture half-length and number of wells. Tang and Sheng (2021) investigated the EOR feasibility of immiscible gas injection in the tight oil reservoir, they indicate that it is hard to get profit for the immiscible gas injection method when the formation permeability is under 0.01 mD. Ding et al. (2021) conducted an experimental analysis of the EOR capacity of gas HNP. They applied particles of different sizes of quartz sand to artificially create cores of different permeability (range from 0.2 to 300 mD). The cores were placed in a core holder during the experiment process, and the influence of different permeability and injected gas were evaluated. The experimental results show that $CO_2$ can remove more crude oil from the matrix, and the most influential factor is matrix permeability.

Optimization studies and sensitivity analysis are necessary to maximize the recovery of HNP. Li L. et al. (2016) analyzed the factors affecting the HNP recovery through experimental methods, and the most important parameter is the pressure gradient. Sanchez-Rivera et al. (2015) indicated that applying HNP too early will weaken the income that it can bring while applying too late will affect the net present value of the entire project. In the HNP process, optimization work is vitally important, many studies have put forward standards for it. For instance, Sheng (2017b) used the near-well pressure as the criterion to optimize the injection and production time. He pointed out that when the pressure near the bottom of the well is close to the set maximum injection pressure and minimum production pressure, the development benefits can be maximized. Meanwhile, the necessity of the soaking stage is still inconclusive and needs to be further discussed. Alharthy et al. (2018) evaluated the potential of $CO_2$ injection for enhanced oil recovery in liquid-rich shale reservoirs, they scaled up laboratory results to the field and concluded that the benefit brought by long soaking time is limited. Injected gas can enter pores of different sizes, numerous studies have analyzed the recovery at the pore level. Wei et al. (2019) analyzed the pore-scale oil distribution changes during $CO_2$ and $N_2$ injection, they indicated that $CO_2$ flooding yielded a relatively uniform displacement front and the contributions of both large and small pores to the overall oil recovery varied during $N_2$ and $CO_2$ flooding process. Bai et al. (2019) analyzed the remaining oil distribution after $CO_2$ HNP and proposed that the remaining oil in the cores is mainly distributed in the small and medium pores. However, the pore-scale analysis is not sufficient to verify the main mechanism of the HNP process, and the literature still lacks a portrayal of the spatial distribution of crude oil during HNP, which needs to be further demonstrated to study the EOR mechanism and conduct an optimization study.

Pressure maintenance is one of the important EOR mechanisms of HNP (Sheng, 2015a). However, due to the difference in oil and gas mobility, gas is easier to flow out of deeper formations. Therefore, when the reservoir is fully pressurized, the range of crude oil that can be effectively recovered is limited. To address such issues, we conducted an experimental study of $CO_2$ HNP in Jimsar tight core samples. This paper intends to carry out a mechanistic study through the following two aspects: 1) Soaking time. Is it necessary for soaking during huff-and-puff operations in the tight reservoir? 2) Pressure gradient. With the increase in pressure gradient, where does the additional oil come from? To achieve these purposes, the NMR experimental methods are used to elucidate the spatial distribution of oil saturation during the HNP process. This paper attempts to provide an insight and a reference for the optimization of $CO_2$ HNP in tight oil reservoirs.

## 2. Principles of the NMR experiment

As the HNP progresses, it is important to clarify the distribution status of crude oil in the formation. Nuclear magnetic resonance (NMR) provides an efficient experimental approach for this purpose. Low-field nuclear magnetic resonance uses pore hydrogen-containing fluid as a probe to obtain fluid properties, distribution, and fluid-containing pore information. By applying the radio frequency (RF) field in a pulsed manner and the spin-echo signal in the pulsed NMR, abundant physical properties in the nuclear magnetic relaxation process can be obtained (Liu and Sheng, 2020).

Scanning sequence refers to the set of related parameters such as radiofrequency pulse, gradient field, and signal acquisition time and their arrangement in time sequence (Callaghan, 1993). In this paper, the CPMG and GR-HSE sequence is used to quantitatively analyze the distribution of crude oil in the tight core during the $CO_2$ HNP process. The realized functions are $T_2$, 1D frequency, and MRI.

The CPMG sequence can evaluate the pore distribution characteristics of the core by analyzing the $T_2$ relaxation variation characteristics of the fluid in the porous medium. When the magnetic field gradient is approximately zero, the transverse relaxation time ($T_2$) of the porous media system is only related to the pore structure of the porous media and is mainly affected by the surface relaxation of the system. The $T_2$ can be expressed as follows (Toumelin et al., 2007):

$$\frac{1}{T_2}=\frac{1}{T_{2b}}+\rho_2\frac{S}{V} \tag{1}$$

where $T_{2b}$ is the bulk liquid relaxation time; $\rho_2$ is the surface relaxivity term; and $S/V$ stands for the surface-to-volume ratio.

Lower $S/V$ means a larger pore size. The fluid in the large pore receives little force from the solid surface and has a strong molecular motion, so the signal attenuation is slow, resulting in a larger $T_2$ value.

The GR-HSE sequence is formed by superimposing spatial linear gradient field based on the HSE sequence, which can obtain the spatial distribution of magnetic moment in the core. For a certain nucleus (such as protons), the Larmor frequency is proportional to the strength of the magnetic field. Based on this theory, 1D frequency and 2D MRI of spatial signals can be realized (Hore, 2015). In the 1D frequency function, the magnetic field strength is a linear function of spatial position, and protons in different positions will resonate at the Larmor frequency corresponding to their position. In this way, the resonance frequency is linearly related to the spatial position. Similarly, by applying three mutually perpendicular gradient magnetic fields, the distribution of hydrogen nuclei density in the three-dimensional space can be characterized. The detection signal is mainly affected by three parts: $H^1$ density, $T_1$, and $T_2$. The spatial distribution function of signal intensity is (Bernstein et al., 2004):

$$\rho(x,y,z) = \rho_0(x,y,z) \cdot \exp\left[\frac{-T_E}{T_2(x,y,z)}\right] \cdot \left\{1 - \exp\left[\frac{-T_R}{T_1(x,y,z)}\right]\right\} \quad (2)$$

where $T_E$ is echo time; $T_R$ is the repetition time; $T_1$ is the longitudinal relaxation time.

The main purpose of this part is to obtain the distribution of oil content in the core, so the weights of the $T_2$ and $T_1$ in the imaging results should be minimized. When $T_E$ is relatively small and $T_R$ is particularly large, the weights of $T_1$ and $T_2$ are not prominent, and the weighted image of hydrogen nuclei density is obtained. The main parameters in the NMR experiment are shown in Table 1.

## 3. Experimental

### 3.1. Materials

Tight sandstone plugs were used in this study. They were cut from the Xinjiang Jimsar outcrop. The petrophysical properties of the core were shown in Table 2. Jimsar crude oil was degassed and dehydrated as the experimental oil. The gas source is $CO_2$ with a purity of 99.9%.

### 3.2. Experimental procedures

Injecting $CO_2$ can effectively reduce the viscosity of the liquid hydrocarbon. Fig. 1 shows the viscosity test result of the crude oil with different mole fractions of $CO_2$. When the mole fraction of $CO_2$ is injected up to 50%, the viscosity of crude oil decreases by 75%, and the viscosity of crude oil decreases slightly when the molar fraction of $CO_2$ continues to increase.

The experimental process consists of four parts: determination of porosity and permeability, core saturation, gas injection test, and NMR scanning. First, the cores were dried and weighed. A PDP (pulse decay permeability) equipment was used to measure the permeability. After that, the core was saturated in the crude oil for 7 days after being fully vacuumed. The saturated core must be weighted after 24 h, which intends to equilibrate the matrix pressure and stabilize the weight. The porosity was determined as the ratio of oil volume to the bulk core volume.

**Table 1**
Key parameters of the NMR experiments.

| Function | Sequences | Field strength, MHz | $T_E$, ms | $T_R$, ms |
|---|---|---|---|---|
| $T_2$ | CPMG | 12 | 0.2 | 3000 |
| 1D frequency | GR-HSE | 12 | 2 | 3000 |
| MRI | GR-HSE | 12 | 4.33 | 400 |

**Table 2**
Core plug properties.

| Core No. | Length, mm | Diameter, mm | Saturated porosity | Permeability, mD |
|---|---|---|---|---|
| R-1 | 50.12 | 25.30 | 0.097 | 0.047 |
| R-2 | 50.23 | 25.42 | 0.088 | 0.058 |
| R-3 | 49.91 | 24.33 | 0.0765 | 0.039 |
| R-4 | 50.17 | 24.56 | 0.082 | 0.066 |

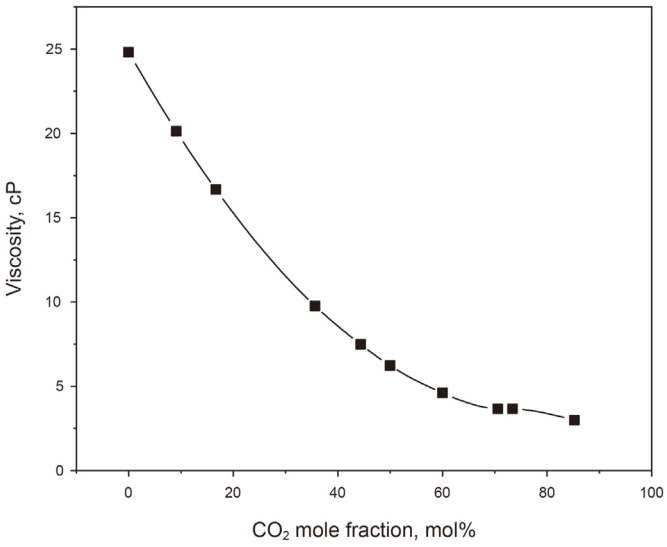


**Fig. 1.** Variation in viscosity of crude oil sample at different $CO_2$ mole frictions.

Unlike flooding, the setup of the injection end and the production end of HNP are the same (Yu et al., 2017). The setup diagram is shown in Fig. 2. HNP procedures are as follows: (1) The core was placed in the core holder, and confining pressure of 13 MPa was applied. (2) Huff: switch T1 was opened and T2 was closed. $CO_2$ was injected from the injection end under the setting injection pressure of 10 MPa. Pressure changes at the injection and close ends of the core were collected to the data acquisition system. When the close end pressure reaches 10 MPa, the core is fully pressurized. At this time, close the injection end. (3) Soaking: switch T1 was closed. (4) Puff: switch T2 was opened to make oil and gas flow out. (5) The core was then taken out, weighed three times, and then averaged. Subsequently, the core was placed in the low-field NMR instrument for scanning. (6) Repeat steps (2)–(5) for more cycles.

In this paper, a complete HNP process consists of several cycles, NMR scanning is required after each cycle. In this process, two curves and one image can be obtained, which are the $T_2$ spectra curve, 1D frequency coding curve, and 2D image. The detailed operation parameters were shown in Table 3. The recovery characteristic of different injection pressure and soaking time was investigated experimentally, while other parameters like injection rate etc. were not the focus of this study.

## 4. Results and discussion

### 4.1. Effect of soaking time

The total operation time for a single cycle is 20–40 min, including 5-min injection, 10-min (or 20-min) soaking (if required), and 15-min production. The pressure change during the first cycle of test R-1 is shown in Fig. 3. After 5 min of injection, the close pressure reached 10 MPa, which indicates that the core was fully pressurized, and the huff stage was ended. After that, the pump was

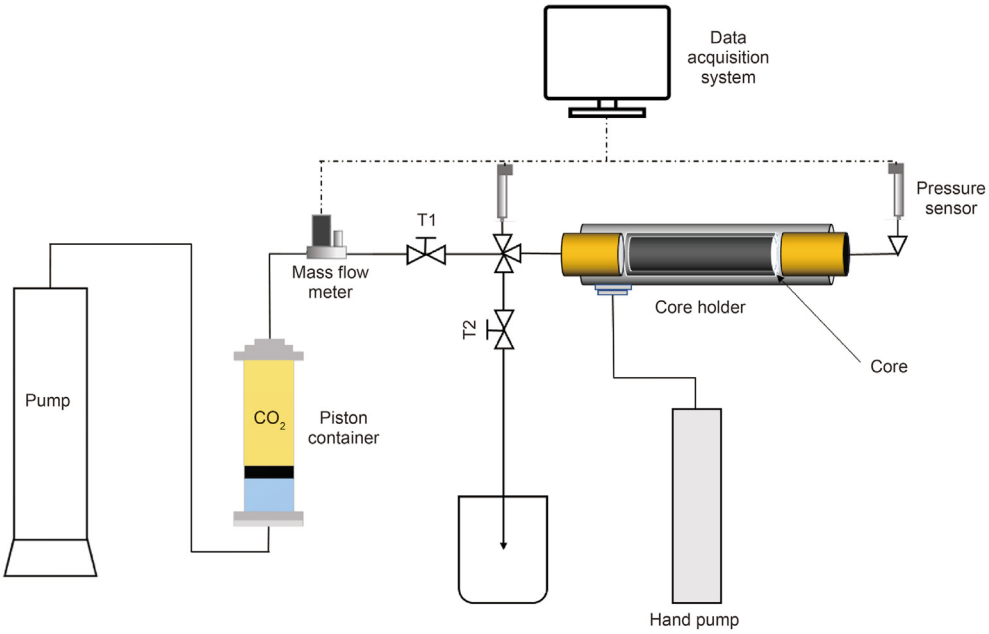


**Fig. 2.** Schematic diagram of $CO_2$ HNP.

**Table 3**
Operating parameters of $CO_2$ HNP tests.

| Test No. | Permeability, mD | Injection pressure, MPa | Injection time, min | Soaking time, min | Production time, min | Cycle |
|---|---|---|---|---|---|---|
| R-1 | 0.047 | 10 | 5 | 10 | 15 | 4 |
| R-2 | 0.058 | 10 | 5 | 0 | 15 | 6 |
| R-3 | 0.039 | 10 | 5 | 20 | 15 | 3 |
| R-4 | 0.066 | 7 | 5 | 10 | 15 | 4 |

closed, soaking for 10 min. Finally, the injection end was opened, and the pressure at the injection end dropped rapidly. After about 15 min, the close end pressure dropped to atmospheric pressure, which indicates the pressure has been fully released.

The oil content is proportional to the signal peak area, so the recovery can be determined by the area difference of the $T_2$ spectra (Liu and Sheng, 2019; Mitchell et al., 2013). In this paper, the recovery factor was measured by both the weighing method and the $T_2$ spectra method. For the weighting method, the core must be weighted after each cycle of production, and the recovery factor ($R$) was calculated by Eq. (3). Where $W_d$ is the weight of dried core; $W_s$ is the weight of oil-saturated core; $W_i$ is the weight of the core after $i$ cycles of production, the detailed information is presented in Table 4. For the $T_2$ spectra method, the $T_2$ spectra of the core are measured before and after each cycle of HNP. The recovery factor is calculated by Eq. (4). $A_i$ is the amplitude of saturated core at different $T_2$; $A_j$ is the amplitude of the core after $j$ cycle of production. The integral represents the area enclosed by the $T_2$ curve and the abscissa.

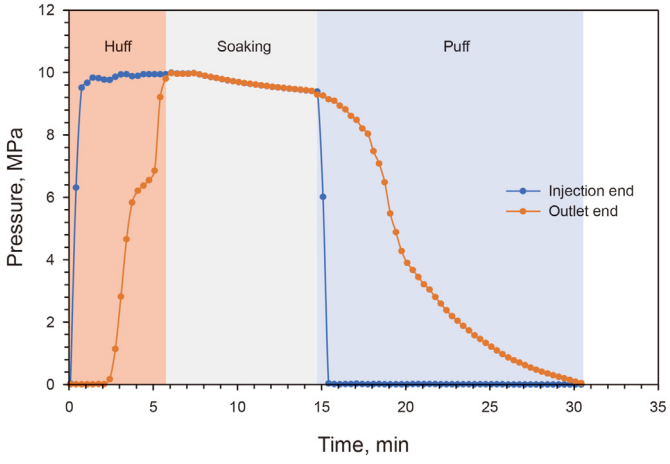


**Fig. 3.** Pressure change during the first cycle of test R-1.

$$R = \frac{W_s - W_i}{W_s - W_d} \tag{3}$$

$$R = \frac{\int_{T_{2min}}^{T_{2max}} (A_i - A_j)\,dT_2}{\int_{T_{2min}}^{T_{2max}} A_i\,dT_2} \tag{4}$$

Figs. 4–6 show the cumulative recovery of tests R-1, R-2, and R-3. The error of the two methods is less than 5%, indicating that NMR can accurately determine recovery under such core conditions (0.6152 g oil-saturated).

The NMR $T_2$ distributions of test R-1 during the $CO_2$ HNP process are present in Fig. 7. The black curve represents the oil distribution of the saturated core. According to the bimodal distribution of $T_2$ spectra, the pore size is divided into small pores ($T_2 < 2.65$ ms) and large pores (2.65 ms $< T_2 <$ 533 ms). The right wave crest is higher

**Table 4**
Weight during the $CO_2$ HNP process.

| Test No. | $W_d$, g | $W_s$, g | $W_1$, g | $W_2$, g | $W_3$, g | $W_4$, g | $W_5$, g | $W_6$, g |
|---|---|---|---|---|---|---|---|---|
| R-1 | 59.4456 | 60.0177 | 59.9010 | 59.8701 | 59.8541 | 59.8341 | 59.8255 | 59.8015 |
| R-2 | 59.7137 | 60.1765 | 60.0779 | 60.0539 | 60.03442 | 60.0233 | – | – |
| R-3 | 59.0299 | 59.6871 | 59.5321 | 59.5033 | 59.4786 | – | – | – |

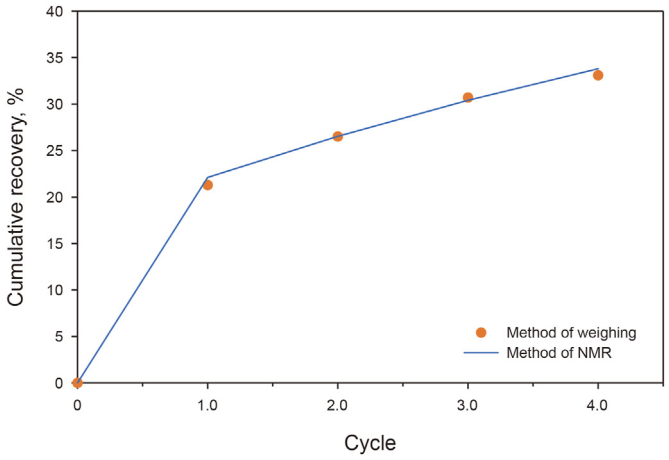


**Fig. 4.** Cumulative recovery of test R-1.

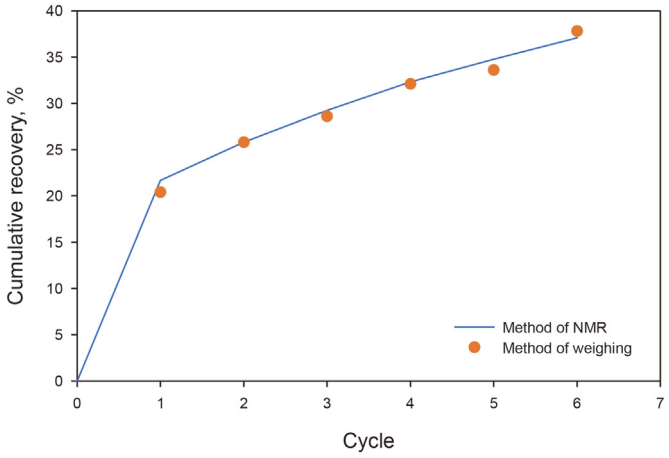


**Fig. 5.** Cumulative recovery of test R-2.

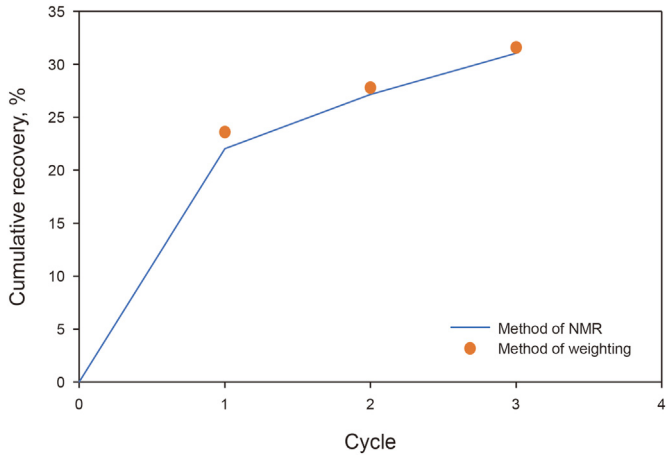


**Fig. 6.** Cumulative recovery of test R-3.

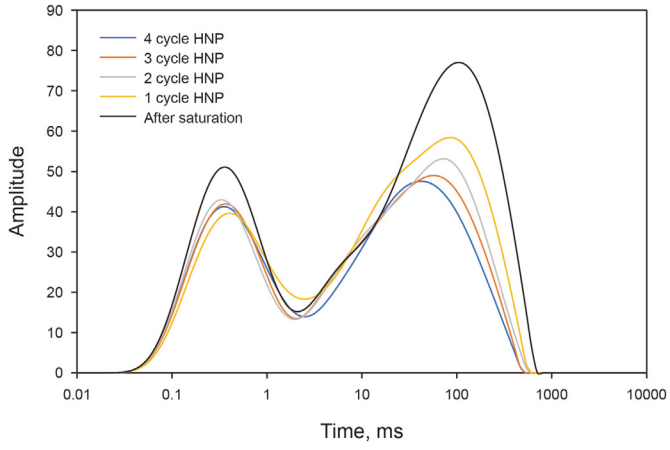


**Fig. 7.** NMR $T_2$ spectra of test R-1 during $CO_2$ HNP.

than the left wave crest, about 70% of the crude oil is distributed in large pores with a relaxation time of 2.65–533 ms, and 30% in small pores with a relaxation time of 0.01–2.65 ms. During the HNP process, the first cycle has the highest recovery, and the production of each cycle gradually decreases as the cycle progresses. For test R-1, the final recovery is 33.8%. The oil produced is mainly from large pores, about 41.50% of the OOIP (original oil in place) in the large pores is recovered, while the oil in the small pores is recovered to a lower degree of 14.28%. As shown by the blue curve, although the oil recovered in the large pores is higher than that in the small pores, the peak area of the large pores is still larger than that of the small pores, most of the remaining oil is still distributed in the large pores. The gas saturation in the core gradually increases at the end of the huff stage, the mobility of gas is much higher than oil, and most of the injected pressure is released in the form of gas flow during the puff stage, which deteriorates the recovery efficiency of oil.

In test R-1, the local oil spatial distributions before and after production are shown in Figs. 8 and 9. In the 2D image, lighter color represents higher oil saturation, and with more cycles conducted, the effective signal becomes darker. The results of the 1D frequency coding and 2D image are in good agreement. The effective signal region representing the oil distribution in the core is located in the middle of the curve with a high amplitude. The noise signal area is distributed at both ends, and the amplitude is much lower. Due to the heterogeneity of the core, the distribution of crude oil in the core after saturation is not uniform. After $CO_2$ HNP, the oil saturation drops significantly. The recovery efficiency of the core injection end is extremely obvious at the end of the 4th cycle, and there exists an almost fully recovered area.

The 1D spatial distribution of the $H^1$ signal during test R-1 is shown in Fig. 10. According to the variation degree of signal amplitude during the HNP process, the core is divided into two regions: hardly movable area and movable area, and the distance

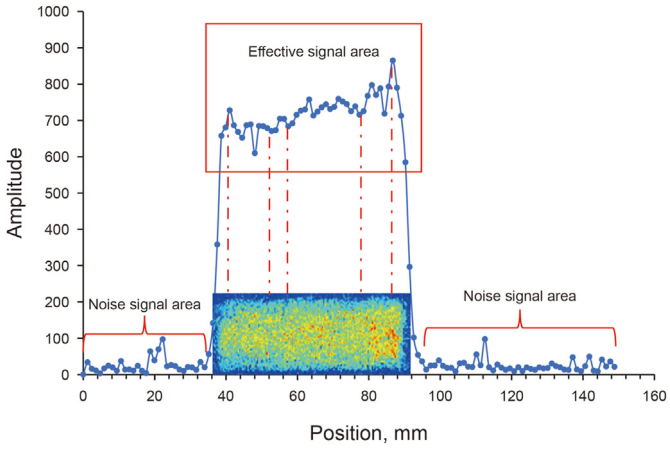


**Fig. 8.** 1D and 2D oil distribution before HNP.

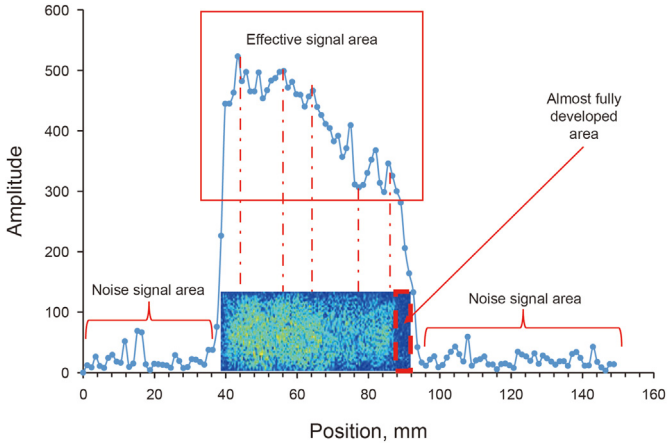


**Fig. 9.** 1D and 2D oil distribution after HNP.

between the junction of the two areas and the injection end is defined as the efficient movable distance. Compared with the movable area, the amplitude decrease of the hardly movable area is less than 10%, and the crude oil distribution trend does not change significantly. Meanwhile, the slope of the trend line of the movable area gradually increases with the cycles, indicating that the effect of crude oil degassing gradually increases as more cycles are conducted. After the end of the first cycle, the overall signal decreases significantly, and the signal amplitude decreases evenly in the core length direction, with no obvious difference in recovery efficiency. With further cycles conducted, the amplitude of the hardly movable area decreases slightly, and the change in oil saturation is not obvious. On the contrary, the signal amplitude in the movable area decreases significantly, suggesting that after the first cycle, the most noticeable reduction of remaining oil saturation occurs in the movable area. After 4 cycles of HNP, the recovery efficiency near the injection end is better, and the efficient movable distance is 32 mm (from 60 to 92 mm), while the crude oil within 18 mm from the close end of the core is difficult to be recovered. From the 2nd cycle, the signal amplitude near the injection end slightly decreases, and the oil saturation in the center of the core decreases significantly. At this time, the main oil produced comes from the center of the core. There are two main reasons for the gradual decrease in recovery efficiency with further cycles conducted: (1) The recoverable crude oil in the movable area is decreased. (2) As the HNP progresses, most of the remaining oil is located in the hardly movable area, which is hard to flow out of the core, resulting in a limited reduction in oil saturation.

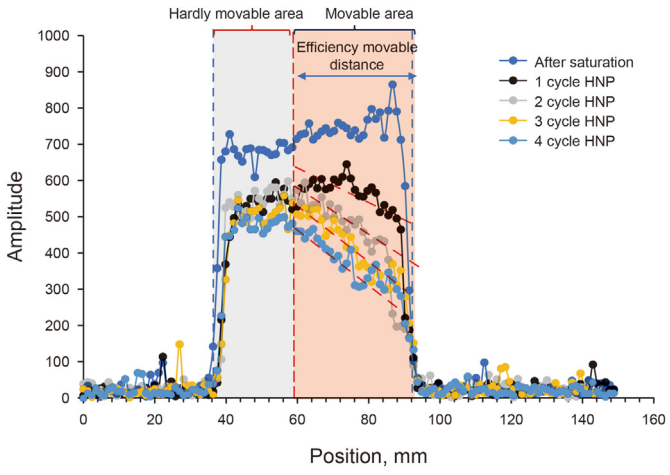


**Fig. 10.** 1D oil distribution of test R-1 during HNP process.

To further visualize the oil distribution during the HNP process, the 2D transverse images of the core were obtained by MRI function (Fig. 11). The brightness of the NMR images represents the oil content, and the part enclosed by the brown dashed line in the figure represents the effective signal of the core. As the HNP progresses, the effective signal becomes weaker, indicating that crude oil is produced gradually. During this process, the 1st cycle has the highest oil production and the most significant signal drops. At the end of the 2nd cycle, the recovery efficiency of the injection end was better than the other parts and has a weaker signal. Such phenomenon is also verified in the third and fourth cycles, the hue on the right side of the core tends to be blue, indicating that the oil has been effectively recovered. Two areas with obvious recovery differences are separated by a red dashed line. As more cycle conducted, the dashed line moves towards the close end of the core. During the HNP process, the effluent hydrocarbon is divided into two parts: one part is dispersed in gaseous $CO_2$ and flows out in the gas phase, and the other part is produced as liquid oil. $CO_2$ can fully interact with the crude oil at the injection end, and this advantage is amplified during the soaking stage. Meanwhile, as $CO_2$ dissolves in the crude oil, the viscosity of the liquid oil decreases, and the flow resistance is reduced.

Test R-2 was conducted to investigate the effect of soaking time on recovery. In test R-2, the soaking time is set to 0, and 6 cycles can be performed under the same operation time. Fig. 12 depicts the $T_2$ spectra inversion data of test R-2. After 6 cycles of HNP, the final recovery was 37.06%, which was higher than test R-1. About 55.52% of the oil in the large pores was recovered, while the crude oil in the small pores was recovered to a lower degree of 21.41%. In this process, the recovery was 32.29% at the end of the fourth cycle, 40.58% of crude oil in large pores was recovered, while that in small pores was 11.67%. In test R-2, the spatial distributions of NMR signals of the core before and after HNP are shown in Fig. 13 and14. After 6 cycles of HNP, the overall signal intensity of the core has dropped significantly. The middle and injection end of the core was well produced, and most of the remaining oil is distributed at the close end.

The 1D spatial distribution of the oil saturation during test R-2 is shown in Fig. 15. It is clearly observed that the movable area of test R-2 is larger, with an efficient movable distance of 37 mm (from 55 to 92 mm). This means more cycles help to effectively develop deeper oil. In contrast to test R-1, the additional recovery of R-2

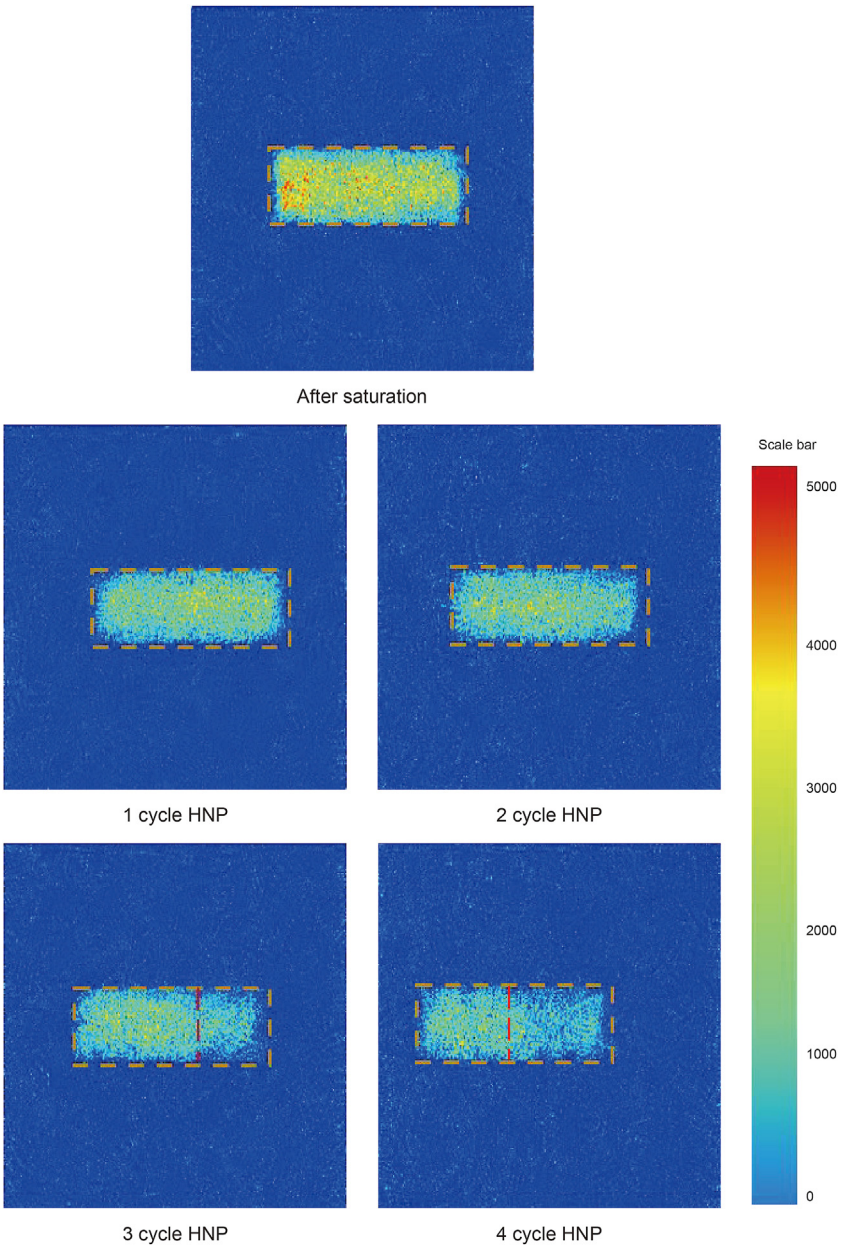


**Fig. 11.** 2D oil distribution during HNP process.

mainly comes from two parts: a larger movable area, and a more thorough recovered effect in the movable area. With two additional cycles conducted, the core was recharged twice and this part of energy in the form of oil and gas production was released. Therefore, it is recommended to perform more cycles in a fixed period of time compared to applying too long soaking stage per cycle. This conclusion is also confirmed by Sheng (2017b) and Sanchez-Rivera (Sanchez-Rivera et al., 2015) by the field-scale simulation approach.

The 2D oil distribution during the HNP process of test R-2 is shown in Fig. 16. Compared with the 1D frequency curve, the 2D image provides a more intuitive view of the recovery differences along the core length direction. The most obvious decline in the first cycle and the overall oil saturation tend to change synchronously during the first three cycles, there is no obvious recovery difference in the core length direction. From the 4th cycle, the difference between the close end and the rest of the core begins to show up. Unlike test R-1, the oil saturation at the injection end does not show too much difference from other areas. Most of the remaining oil is distributed at the close end, and the oil near the injection end is efficiently recovered.

To further investigate the effect of soaking on recovery efficiency, test R-3 was conducted. Unlike test R-1, test R-3 has a longer soaking time (20 min) to ensure that the pressure in the core is fully balanced, and pressure equalization at both ends of the core after 17 min of soaking (Fig. 17).

The $T_2$ spectra distribution of test R-3 is shown in Fig. 18. After three cycles of HNP, 35.81% of the oil in the large pores was recovered, while the crude oil in the small pores was recovered to a lower degree of 16.06%. For a more visual comparison of the recovery efficiency under different soaking time scenarios, the crude oil recovery values under different pore sizes of tests R-1, R-2, and R-3 are depicted in Fig. 19. When the cycle is the same (3 cycles),

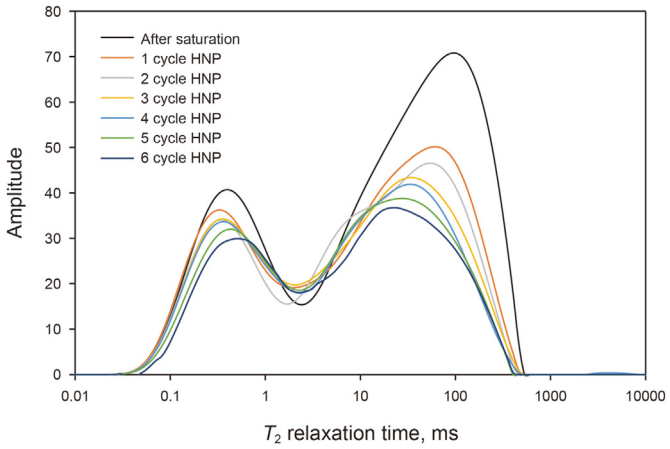


**Fig. 12.** NMR $T_2$ spectra of test R-2 during $CO_2$ HNP.

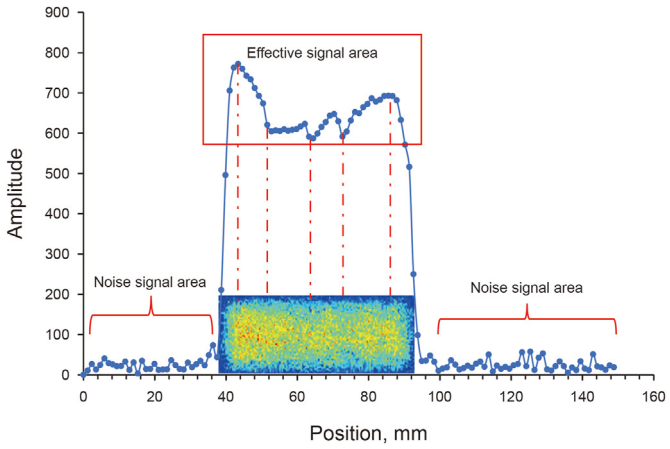


**Fig. 13.** 1D and 2D oil distribution before HNP.

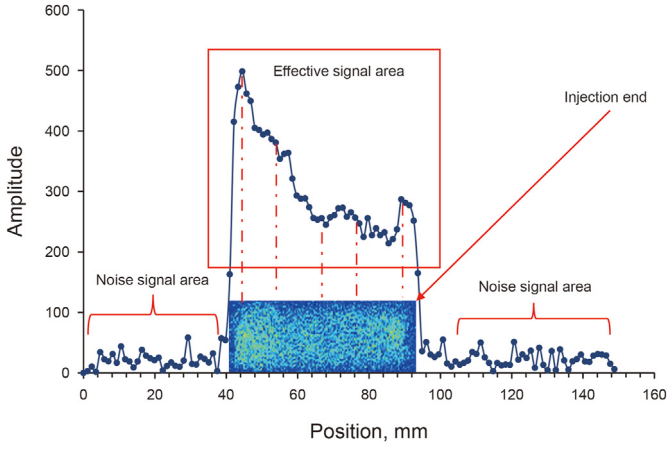


**Fig. 14.** 1D and 2D oil distribution after HNP.

test R-3 shows a higher total recovery, suggesting that longer soaking time leads to higher recovery with the same HNP cycle operated. Meanwhile, after 3 cycles of HNP, the total recovery of test R-1 (10-min soaking, light orange bar in Fig. 19) is 30.4%, which is similar to test R-3 (purple bar). Such a result indicates too long soaking time contributes little to the increase in total recovery.

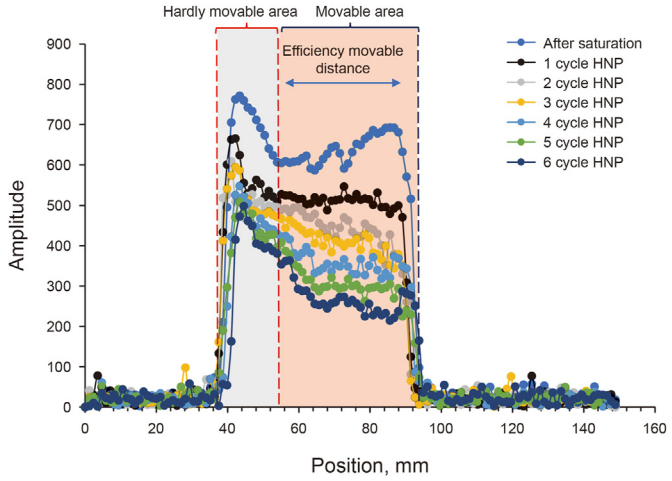


**Fig. 15.** 1D oil distribution of test R-2 during HNP process.

From a microscopic perspective, soaking helps both improve the recovery of small pores and large pores. Compared with small pores, soaking has less impact on the production of crude oil in large pores. After three cycles of HNP, the recovery values from the small pores of tests R-1, R-2, and R-3 are 13.21%, 11.87%, and 16.06%, respectively. However, such a difference is not reflected in the total recovery, and the total recovery is more relevant to the recovery of the large pores, which means the recovery of the small pore is not the determinant of the total recovery. Compared with soaking, applying additional cycles of HNP is able to recover more oil from the pores. After 6 cycles of HNP, test R-2 could recover more oil from both large pores and small pores, and the final recovery is highest.

The 1D and 2D distributions of test R-3 are shown in Figs. 20 and 21. Similar to tests R-1 and R-2, the core is divided into the hardly movable area and movable area, and the efficient movable distance of test R-3 is 25 mm (from 80 to 105 mm), which is smaller than that of tests R-1 and R-2.

Molecular diffusion, viscosity reduction, dissolved gas drive, and pressure maintenance are the main mechanisms of $CO_2$ HNP in tight reservoirs (Alfarge et al., 2018; Hoffman and Rutledge, 2019; Sanchez-Rivera et al., 2015; Yu et al., 2015). In the injection stage, $CO_2$ can enter the matrix by both advection and diffusion. While in the soaking stage, reservoir pressure tends to stabilize, and diffusion becomes the dominant mode of gas transfer. Numerous studies have concluded that gas penetrates deeper into the reservoir and fully interacts with the formation fluids during the soaking stage (Alfarge et al., 2018; Hoffman and Rutledge, 2019; Sanchez-Rivera et al., 2015). However, according to the experiments conducted by Li S. et al. (2018), the diffusion coefficient magnitude of $CO_2$ in oil-saturated porous media is $10^{-10}$ $m^2/s$. With such a low diffusion coefficient, the amount of the $CO_2$ that can penetrate into the formation in the soaking stage is limited. At the same time, as we demonstrated above, even if the pressure (gas) can sweep to the deep reservoir, this part of crude oil may not be able to be effectively recovered. In this experiment, crude oil in the range of 25–39 mm can be effectively developed. It is reasonable to believe that in the field-scale, the effective movable area by HNP in the tight reservoir is also limited, and the movable area mainly depends on the stimulated reservoir volume (SRV) (Li Li et al., 2018).

In general, soaking does play an important role in the HNP process, which helps to better recover the oil from pore medium, especially in small pores. However, more oil is found in the large pores, which is easier to recover. As we mentioned above, even after

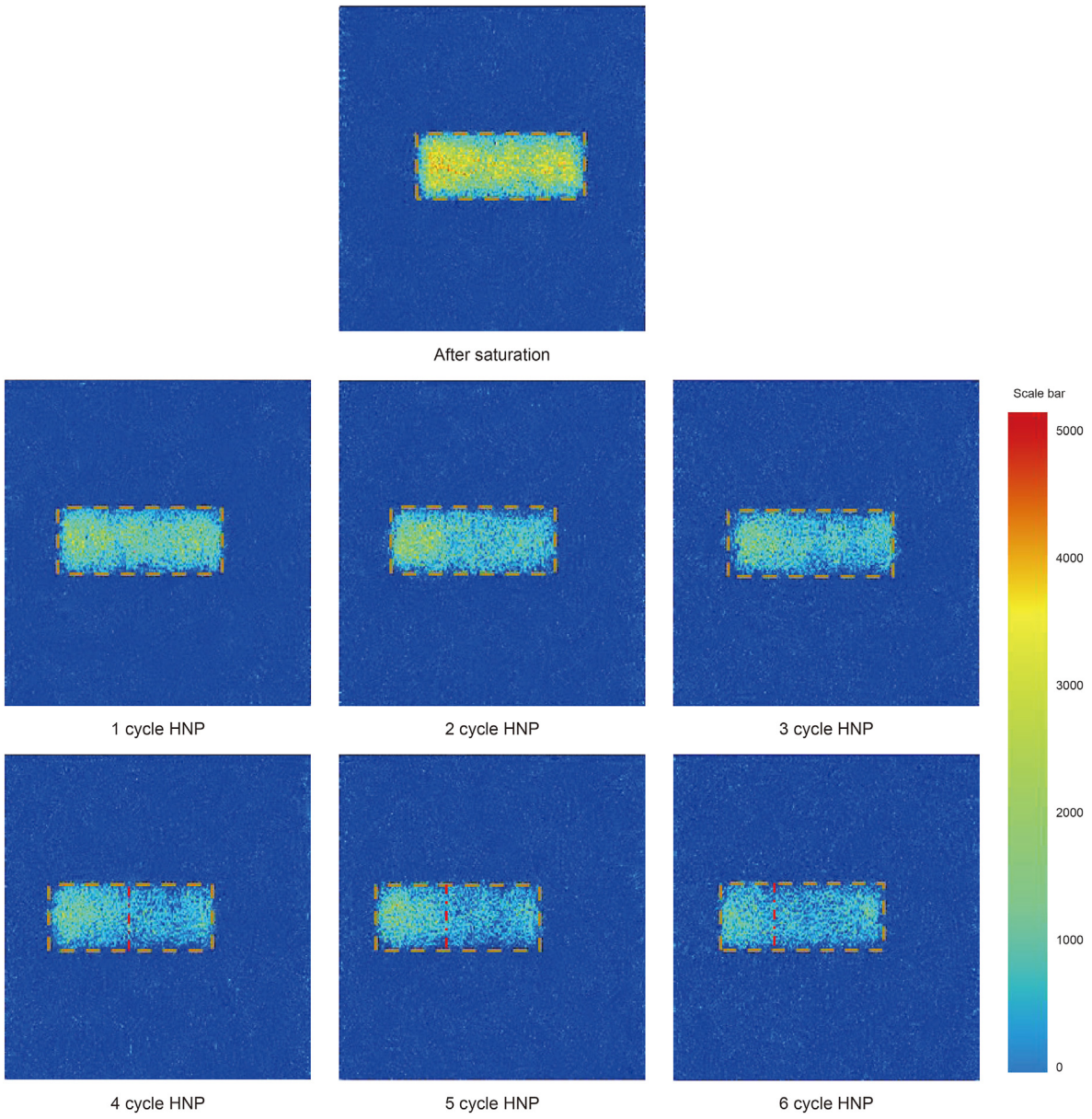


**Fig. 16.** 2D oil distribution of test R-2 during HNP process.

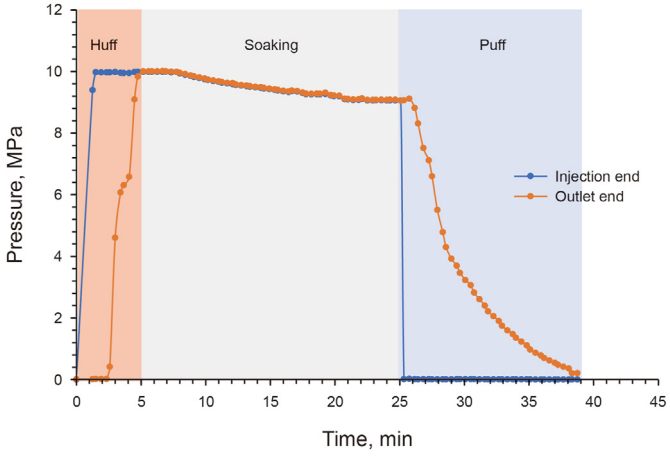


**Fig. 17.** Pressure change during the first cycle of test R-3.

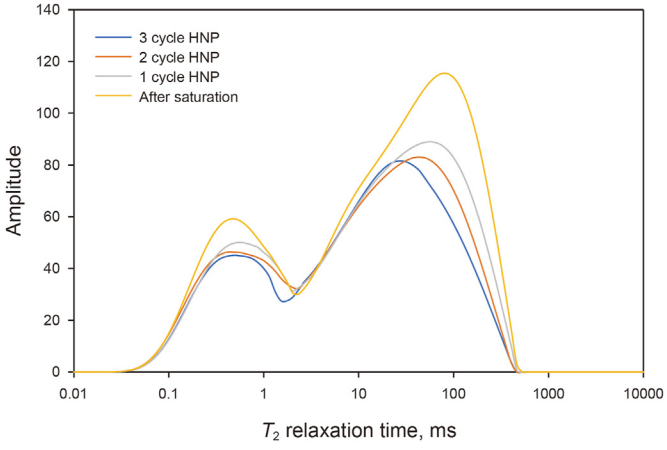


**Fig. 18.** NMR $T_2$ spectra of test R-3 during $CO_2$ HNP.

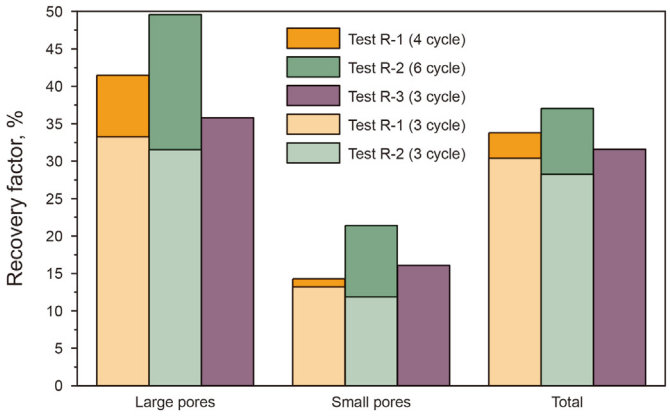


**Fig. 19.** Pore-scale recovery efficiency of tests R-1, R-2, and R-3.

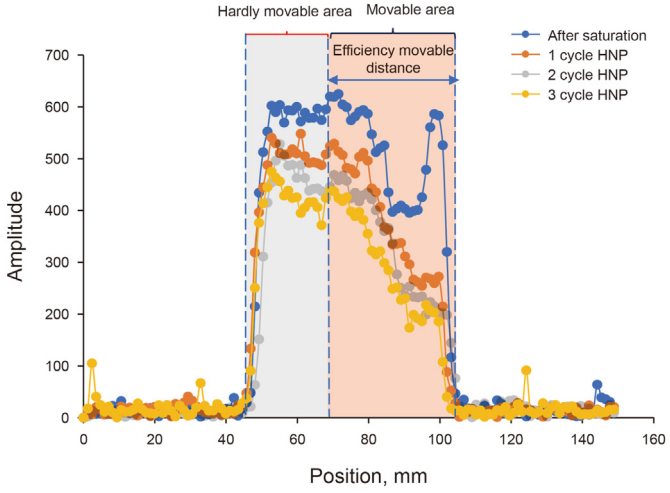


**Fig. 20.** 1D oil distribution of test R-3 during HNP process.

several cycles of HNP, the recovery efficiency of small pores is still limited. From a microscopic point of view, the main target of $CO_2$ HNP is the oil located in the large pores, while performing more cycles helps to extract more oil from large pores and deeper formation. Therefore, more cycles are recommended instead of applying too long soaking time.

### 4.2. Effect of pressure gradient

The injection and production pressures determine the pressure gradient, which affects the effect of HNP in many aspects. As the driving force of gas into the core, the injection pressure directly affects the velocity of gas penetration in the oil-saturated porous media, thus affecting the gas penetration depth and the degree of interaction between oil and gas. During the soaking process, the higher soaking pressure promotes more $CO_2$ to dissolve into the crude oil, which increases the elastic energy of the fluid and further reduces the viscosity of the crude oil. As the pressure decreases in the production stage, the crude oil degasses, and oil is driven out of the core.

Test R-4 was conducted to investigate the influence of pressure gradient on $CO_2$ HNP. The injection pressure of test R-4 is 7 MPa, and the operation time of injection, soaking, and production are the same as test R-1 with the injection pressure being 10 MPa.

Fig. 22 depicts the $T_2$ spectrum inversion data of test R-4. In line with earlier results, the 1st cycle shares the highest recovery, 17.49% of OOIP was recovered during this process. As more cycles proceeded, the recovery efficiency gradually decreased, the cycle recovery was 4.51%, 3.29%, and 2.50%, respectively, and 27.79% of the oil was recovered after 4 cycles of production. According to the area change of the bimodal curve, the recovery efficiency of crude oil in the large and small pores during the HNP process is clarified. To further illustrate the influence of different injection pressures on the recovery efficiency, the crude oil recovery efficiency under different pore sizes ($T_2$) of tests R-1 and R-4 is summarized in Fig. 23. Changes in pressure gradient have a significant impact on development efficiency. With the decrease in injection pressure, the recovery factor of crude oil in large pores and small pores decreased by 6.12% and 4.81% respectively, and the total recovery decreased by 5.51%.

Fig. 24 presents the 1D spatial distribution of oil saturation during test R-4. The contribution of different locations to the production can be readily distinguished by the decrease in magnitude. The average amplitude gradually decreases as the cycle progresses. Besides, the movable area of test R-4 is smaller, and the efficient movable distance is 24 mm (from 68 to 92 mm). Increasing the pressure gradient facilitates the expansion of the movable area, which can effectively recover crude oil from the deeper formation.

During the huff stage, part of the injected gas is dissolved in the crude oil, and the other part is distributed in the pore space in the form of free gas, which effectively increases the core pressure. In the puff stage, the production characteristics are similar to the solution gas drive. In the dissolved gas drive process, once the formation pressure drops below the bubble point pressure, the crude oil deep in the formation degasses, resulting in a decrease in production and a rapid increase in the gas-to-oil ratio. As for the HNP process, as the oil is saturated with $CO_2$ after the huff stage, the injection pressure is the bubble point pressure, thus the degassing of the oil occurs throughout the puff stage. For the hardly movable area, the crude oil needs to be transported a long distance to reach the production end. In this process, the crude oil is rapidly degassed, and most of the pressure is released in the form of gas flow, which deteriorates the oil recovery efficiency of the hardly movable area.

## 5. Summary and conclusions

In the present paper, we compared the recovery efficiency at different soaking times and pressure gradients by the NMR method. Through analyzing the change of spatial distribution of oil saturation during the HNP process, the mechanisms of $CO_2$ HNP in tight reservoirs are discussed. The main conclusions reached in this study are as follows.

(1) $CO_2$ HNP can effectively improve the recovery of tight reservoirs. The produced oil is mainly from the large pores, and most of the remaining oil still exists in the large pores after the HNP process.
(2) The spatial distribution of crude oil in the formation during the HNP process is similar to that of the dissolved gas drive. For crude oil in the deep part of the formation, it has to travel a long distance to reach the producer, during which the oil degasses and severely reduces the ability of deep oil to flow out, resulting in a large amount of residual oil distributed in the deep part of the formation. Therefore, the dissolved gas

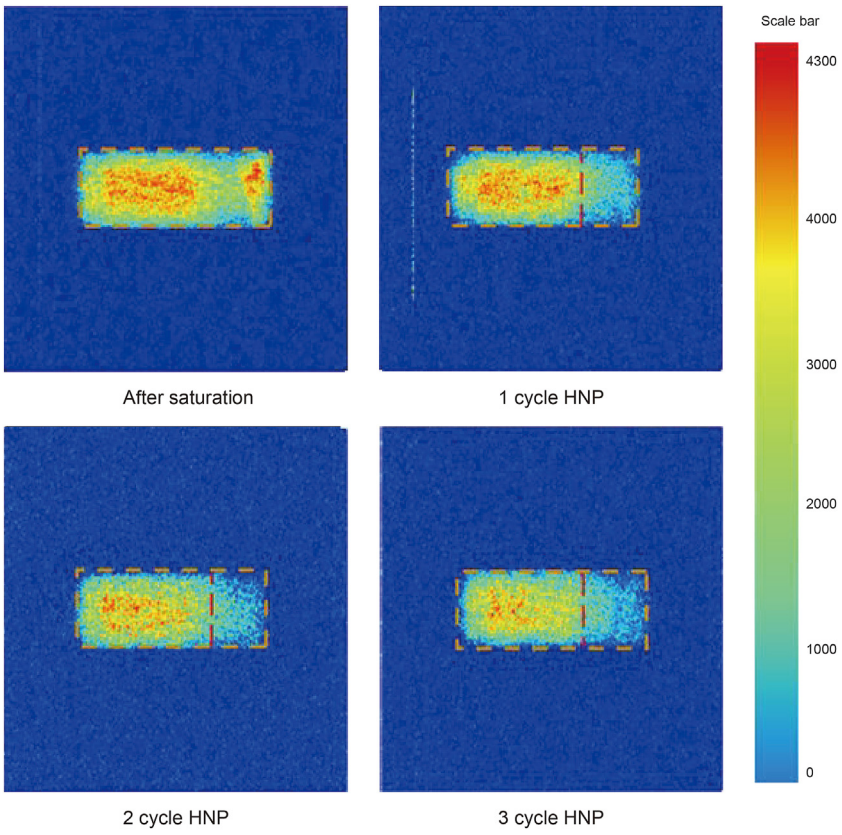


**Fig. 21.** 2D oil distribution of test R-3 during HNP process.

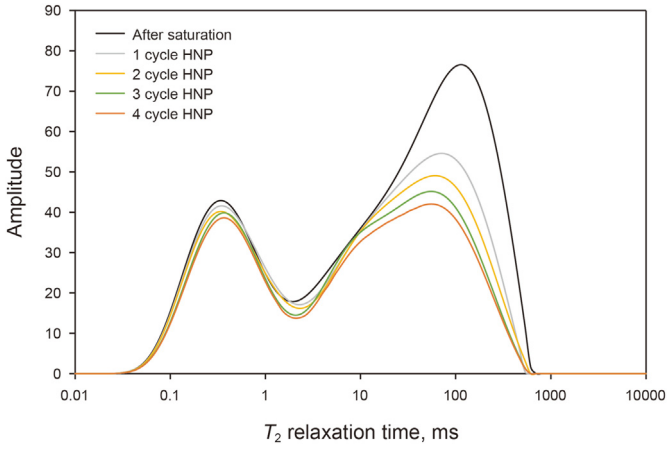


**Fig. 22.** NMR $T_2$ spectra of test R-4 during $CO_2$ HNP.

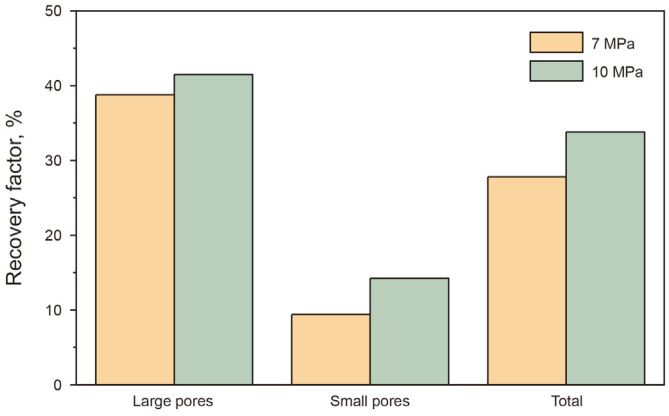


**Fig. 23.** Pore-scale recovery efficiency of tests R-1 and R-4.

drive is considered to be a crucial EOR mechanism of $CO_2$ huff-n-puff.

(3) The depth of crude oil that can be effectively recovered by HNP is limited, and more cycles conducted help to recover deeper oil in the tight formation. In the cases studied in this paper, the oil in the depth range of 25–39 mm can be effectively exploited after 3–6 cycles HNP.

(4) The necessity of soaking in tight reservoirs is questionable. A soaking-containing cycle shares a higher recovery in a single cycle, and higher recovery efficiency in small pores is achieved. Nevertheless, without applying the soaking stage may reduce the operation time per cycle, resulting in more cycles conducted over a fixed period of time, which can significantly increase the effective movable area, and achieve higher total recovery. Therefore, shorter soaking times even no soaking stage is suggested in the tight reservoir.

(5) More oil comes out of the matrix with the increase in injection pressure. Increased injection pressure helps to expand the movable area and thus more effectively recover crude oil from deeper in the formation.

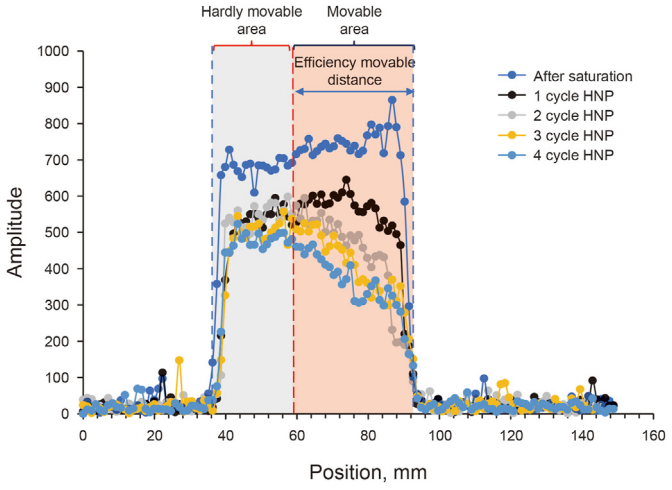


**Fig. 24.** 1D oil distribution of test R-4 during HNP process.

## Acknowledgments

The work is supported by the Strategic Cooperation Technology Projects of CNPC and CUPB (ZLZX2020) and by the Fundamental Research Funds for the Central Universities of China.

## References

Abedini, A., Torabi, F., 2014. On the $CO_2$ storage potential of cyclic $CO_2$ injection process for enhanced oil recovery. Fuel 124, 14–27. https://doi.org/10.1016/j.fuel.2014.01.084.

Alfarge, D., Wei, M., Bai, B., 2018. $CO_2$-EOR mechanisms in huff-n-puff operations in shale oil reservoirs based on history matching results. Fuel 226, 112–120. https://doi.org/10.1016/j.fuel.2018.04.012.

Alharthy, N., Teklu, T., Kazemi, H., et al., 2018. Enhanced oil recovery in liquid–rich shale reservoirs: laboratory to field. SPE Reservoir Eval. Eng. 21 (1), 137–159. https://doi.org/10.2118/175034-PA.

Bachu, S., 2016. Identification of oil reservoirs suitable for $CO_2$-EOR and $CO_2$ storage (CCUS) using reserves databases, with application to Alberta, Canada. Int. J. Greenh. Gas Control 44, 152–165. https://doi.org/10.1016/j.ijggc.2015.11.013.

Bai, H., Zhang, Q., Li, Z., et al., 2019. Effect of fracture on production characteristics and oil distribution during $CO_2$ huff-n-puff under tight and low-permeability conditions. Fuel 246, 117–125. https://doi.org/10.1016/j.fuel.2019.02.107.

Bernstein, M.A., King, K.F., Zhou, X.J., 2004. Handbook of MRI Pulse Sequences. Elsevier, Oxford.

Callaghan, P.T., 1993. Principles of Nuclear Magnetic Resonance Microscopy. Oxford University, Oxford.

Chen, C., Balhoff, M., Mohanty, K.K., 2014. Effect of reservoir heterogeneity on primary recovery and $CO_2$ huff 'n'puff recovery in shale-oil reservoirs. SPE Reserv. Eval. Eng. Sci. 17 (3), 404–413. https://doi.org/10.2118/164553-PA.

Cuéllar-Franca, R.M., Azapagic, A., 2015. Carbon capture, storage and utilisation technologies: a critical analysis and comparison of their life cycle environmental impacts. J. $CO_2$ Util. 9, 82–102. https://doi.org/10.1016/j.jcou.2014.12.001.

Ding, M., Wang, Y., Liu, D., et al., 2021. Enhancing tight oil recovery using $CO_2$ huff and puff injection: an experimental study of the influencing factors. J. Natural Gas Sci. Eng. Sci. 90, 103931. https://doi.org/10.1016/j.jngse.2021.103931.

Duan, Q., Yang, X., 2014. Experimental studies on gas and water permeability of fault rocks from the rupture of the 2008 Wenchuan earthquake, China. J. Sci. China Earth Sci. 57 (11), 2825–2834. https://doi.org/10.1007/s11430-014-4948-7.

Hoffman, B.T., Rutledge, J.M., 2019. Mechanisms for Huff-n-Puff cyclic gas injection into unconventional reservoirs. SPE Oklahoma City Oil and Gas Symposium. https://doi.org/10.2118/195223-MS.

Hore, P.J., 2015. Nuclear Magnetic Resonance. Oxford University Press, USA.

Li, L., Sheng, J.J., Sheng, J., 2016. Optimization of huff-n-puff gas injection to enhance oil recovery in shale reservoirs. SPE Low Perm Symposium. https://doi.org/10.2118/180219-MS.

Li, L., Su, Y., Sheng, J.J., 2018. Investigation of gas penetration depth during gas huff-n-puff EOR process in unconventional oil reservoirs. In: SPE Canada Unconventional Resources Conference. https://doi.org/10.2118/189804-MS.

Li, Q., Chen, A., Zhang, T., et al., 2016. Positioning and revision of CCUS technology development in China. Int. J. Greenh. Gas Control 46, 282–293. https://doi.org/10.1016/j.ijggc.2015.02.024.

Li, S., Qiao, C., Zhang, C., Li, Z., 2018. Determination of diffusion coefficients of supercritical $CO_2$ under tight oil reservoir conditions with pressure-decay method. J. $CO_2$ Util. 24, 430–443. https://doi.org/10.1016/j.jcou.2018.02.002.

Liu, J., Sheng, J.J., 2019. Experimental investigation of surfactant enhanced spontaneous imbibition in Chinese shale oil reservoirs using NMR tests. J. Ind. Eng. Chem. 72, 414–422. https://doi.org/10.1016/j.jiec.2018.12.044.

Liu, J., Sheng, J.J., 2020. Investigation of countercurrent imbibition in oil-wet tight cores using NMR technology. SPE J. 25 (5), 2601–2614. https://doi.org/10.2118/201099-PA.

Ma, J., Wang, X., Gao, R., et al., 2015. Enhanced light oil recovery from tight formations through $CO_2$ huff 'n'puff processes. Fuel 154, 35–44. https://doi.org/10.1016/j.fuel.2015.03.029.

Mitchell, J., Staniland, J., Chassagne, R., et al., 2013. Mapping oil saturation distribution in a limestone plug with low-field magnetic resonance. J. Petrol. Sci. Eng. 108, 14–21. https://doi.org/10.1016/j.petrol.2013.04.008.

Pang, Z., Zou, C., Tao, S., et al., 2012. Formation, distribution and resource evaluation of tight oil in China. Eng. Sci. 14 (7), 60–67 (in Chinese).

Qin, J., Han, H., Liu, X., 2015. Application and enlightenment of carbon dioxide flooding in the United States of America. Petrol. Explor. Dev. 42 (2), 232–240. https://doi.org/10.1016/S1876-3804(15)30010-0.

Sanchez-Rivera, D., Mohanty, K., Balhoff, M., 2015. Reservoir simulation and optimization of huff-and-puff operations in the Bakken shale. Fuel 147, 82–94. https://doi.org/10.1016/j.fuel.2014.12.062.

Sheng, J.J., 2015a. Enhanced oil recovery in shale reservoirs by gas injection. J. Nat. Gas Sci. Eng. 22, 252–259. https://doi.org/10.1016/j.jngse.2014.12.002.

Sheng, J.J., 2015b. Increase liquid oil production by huff-n-puff of produced gas in shale gas condensate reservoirs. J. Unconvent. Oil Gas Resour. 11, 19–26. https://doi.org/10.1016/j.juogr.2015.04.004.

Sheng, J.J., 2017a. Critical review of field EOR projects in shale and tight reservoirs. J. Petrol. Sci. Eng. 159, 654–665. https://doi.org/10.1016/j.petrol.2017.09.022.

Sheng, J.J., 2017b. Optimization of huff-n-puff gas injection in shale oil reservoirs. Petroleum 3 (4), 431–437. https://doi.org/10.1016/j.petlm.2017.03.004.

Sheng, J.J., Chen, K., 2014. Evaluation of the EOR potential of gas and water injection in shale oil reservoirs. J. Unconvent. Oil Gas Resour. 5, 1–9. https://doi.org/10.1016/j.juogr.2013.12.001.

Tang, W., Sheng, J., 2021. Huff-n-puff gas injection or gas flooding in tight oil reservoirs? J. Petrol. Sci. Eng. https://doi.org/10.1016/j.petrol.2021.109725, 109725.

Toumelin, E., Torres-Verdín, C., Sun, B., Dunn, K.-J., 2007. Random-walk technique for simulating NMR measurements and 2D NMR maps of porous media with relaxing and permeable boundaries. J. Magn. Reson. 188 (1), 83–96. https://doi.org/10.1016/j.jmr.2007.05.024.

Wei, B., Zhang, X., Wu, R., et al., 2019. Pore-scale monitoring of $CO_2$ and $N_2$ flooding processes in a tight formation under reservoir conditions using nuclear magnetic resonance (NMR): a case study. Fuel 246, 34–41. https://doi.org/10.1016/j.fuel.2019.02.103.

Yu, H., Fu, W., Zhang, Y., et al., 2021. Experimental study on EOR performance of $CO_2$-based flooding methods on tight oil. Fuel 290, 119988. https://doi.org/10.1016/j.fuel.2020.119988.

Yu, W., Lashgari, H.R., Wu, K., Sepehrnoori, K., 2015. $CO_2$ injection for enhanced oil recovery in Bakken tight oil reservoirs. Fuel 159, 354–363. https://doi.org/10.1016/j.fuel.2015.06.092.

Yu, Y., Li, L., Sheng, J.J., 2017. A comparative experimental study of gas injection in shale plugs by flooding and huff-n-puff processes. J. Natural Gas Sci. Eng. Sci. 38, 195–202. https://doi.org/10.1016/j.jngse.2016.12.040.

Zhou, X., Wang, Y., Zhang, L., et al., 2020. Evaluation of enhanced oil recovery potential using gas/water flooding in a tight oil reservoir. Fuel 272, 117706. https://doi.org/10.1016/j.fuel.2020.117706.

Zou, C., Yang, Z., Zhang, G., et al., 2014. Conventional and unconventional petroleum "orderly accumulation": concept and practical significance. Petrol. Explor. Dev. 41 (1), 14–30. https://doi.org/10.1016/S1876-3804(14)60002-1.

Zou, C., Zhai, G., Zhang, G., et al., 2015. Formation, distribution, potential and prediction of global conventional and un-conventional hydrocarbon resources. Petrol. Explor. Dev. 42 (1), 14–28. https://doi.org/10.1016/S1876-3804(15)60002-7.

Zuloaga, P., Yu, W., Miao, J., Sepehrnoori, K., 2017. Performance evaluation of $CO_2$ Huff-n-Puff an-d continuous CO2 injection in tight oil reservoirs. Energy 134, 181–192. https://doi.org/10.1016/j.energy.2017.06.028.